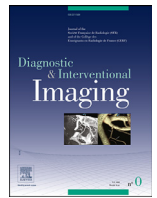




ELSEVIER



Original article/Cardiac imaging

Improved myocardial scar visualization with fast free-breathing motion-compensated black-blood T₁-rho-prepared late gadolinium enhancement MRI



Soumaya Sridi^{a,*}, Marta Nuñez-García^b, Maxime Sermesant^{b,c}, Aurélien Maillot^b,
Dounia El Hamrani^b, Julie Magat^b, Jérôme Naulin^b, François Laurent^a, Michel Montaudon^a,
Pierre Jaïs^{b,d}, Matthias Stuber^{b,e,f}, Hubert Cochet^{a,b}, Aurélien Bustin^{a,b,e}

^a Department of Cardiovascular Imaging, Groupe Hospitalier Sud, CHU Bordeaux, 33000, Pessac, France

^b IHU LIRYC, Electrophysiology and Heart Modeling Institute, Université de Bordeaux, INSERM U1045, 33600, Pessac, France

^c INRIA, Université Côte d'Azur, Sophia Antipolis, 06902, Valbonne, France

^d Department of Cardiac Electrophysiology, Hôpital Cardiologique du Haut-Lévêque, CHU de Bordeaux, 33600, Pessac, France

^e Department of Diagnostic and Interventional Radiology, Lausanne University Hospital and University of Lausanne, 1011, Lausanne, Switzerland

^f Center for Biomedical Imaging (CIBM), 1015, Lausanne, Switzerland

ARTICLE INFO

Keywords:

Gadolinium enhancement
Heart
Magnetic resonance imaging
Myocardial infarction
Motion

ABSTRACT

Purpose: Clinical guidelines recommend the use of bright-blood late gadolinium enhancement (BR-LGE) for the detection and quantification of regional myocardial fibrosis and scar. This technique, however, may suffer from poor contrast at the blood-scar interface, particularly in patients with subendocardial myocardial infarction. The purpose of this study was to assess the clinical performance of a two-dimensional black-blood LGE (BL-LGE) sequence, which combines free-breathing T₁-rho-prepared single-shot acquisitions with an advanced non-rigid motion-compensated patch-based reconstruction.

Materials and methods: Extended phase graph simulations and phantom experiments were performed to investigate the performance of the motion-correction algorithm and to assess the black-blood properties of the proposed sequence. Fifty-one patients (37 men, 14 women; mean age, 55 ± 15 [SD] years; age range: 19–81 years) with known or suspected cardiac disease prospectively underwent free-breathing T₁-rho-prepared BL-LGE imaging with inline non-rigid motion-compensated patch-based reconstruction at 1.5T. Conventional breath-held BR-LGE images were acquired for comparison purposes. Acquisition times were recorded. Two readers graded the image quality and relative contrasts were calculated. Presence, location, and extent of LGE were evaluated.

Results: BL-LGE images were acquired with full ventricular coverage in 115 ± 25 (SD) sec (range: 64–160 sec). Image quality was significantly higher on free-breathing BL-LGE imaging than on its breath-held BR-LGE counterpart (3.6 ± 0.7 [SD] [range: 2–4] vs. 3.9 ± 0.2 [SD] [range: 3–4]) ($P < 0.01$) and was graded as diagnostic for 44/51 (86%) patients. The mean scar-to-myocardium and scar-to-blood relative contrasts were significantly higher on BL-LGE images ($P < 0.01$ for both). The extent of LGE was larger on BL-LGE (median, 5 segments [IQR: 2, 7 segments] vs. median, 4 segments [IQR: 1, 6 segments]) ($P < 0.01$), the method being particularly sensitive in segments with LGE involving the subendocardium or papillary muscles. In eight patients (16%), BL-LGE could ascertain or rule out a diagnosis otherwise inconclusive on BR-LGE.

Conclusion: Free-breathing T₁-rho-prepared BL-LGE imaging with inline motion compensated reconstruction offers a promising diagnostic technology for the non-invasive assessment of myocardial injuries.

© 2022 The Author(s). Published by Elsevier Masson SAS on behalf of Société française de radiologie. This is an open access article under the CC BY license (<http://creativecommons.org/licenses/by/4.0/>)

Abbreviations: 2D, Two-dimensional; 3D, Three-dimensional; ADMM, Alternating direction method of multipliers; BR-LGE, Bright-blood late gadolinium-enhanced; BL-LGE, Black-blood late-gadolinium-enhanced; bSSFP, Balanced steady-state free-precession; CMR, Cardiovascular magnetic resonance; ECG, Electrocardiogram; FIDDLE, Flow-independent dark-blood delayed enhancement; FSL, Spin-lock frequency; GMD, General matrix description; IQR, Interquartile range; NGS, Normalized gradient

squares; ROI, Region of interest; SD, Standard deviation; SI, Signal intensity; SL, Spin-lock; T₁ρ, T₁-rho-prepared; TI, Inversion time; TSL, Spin-lock time

* Corresponding author.

E-mail address: soumayasridi@gmail.com (S. Sridi).

<https://doi.org/10.1016/j.diii.2022.07.003>

2211-5684/© 2022 The Author(s). Published by Elsevier Masson SAS on behalf of Société française de radiologie. This is an open access article under the CC BY license (<http://creativecommons.org/licenses/by/4.0/>)

1. Introduction

Bright-blood late gadolinium-enhanced imaging (BR-LGE) is the cornerstone technique providing cardiac magnetic resonance (CMR) with the largest incremental value as compared with other cardiac imaging modalities [1]. The presence, extent, and distribution of LGE are key features to assess the etiological diagnosis in acute coronary syndromes, chronic structural heart diseases, or ventricular arrhythmias, or to assess the prognosis in patients with structural heart diseases [2,3]. The strength of the technique lies in its ability to provide high contrast between the injured and viable myocardium, thanks to an inversion recovery mechanism that artificially blackens the surrounding healthy tissue in the images [4]. However, while much progress has been made since their introduction more than two decades ago, LGE techniques still share a common drawback: they have been designed to null the healthy myocardium signal without suppressing the blood signal, which often results in poor contrast between the scar and the blood that is present in the adjacent cardiac chambers [5]. This contrast issue makes the analysis of LGE images the most complex step of CMR interpretation and the one associated with the longest learning curve. Furthermore, this limits the sensitivity of LGE CMR to small subendocardial scars within the left ventricular wall or to scars involving thinner walls such as the right ventricle or the atria. Moreover, the poor contrast between scar and blood pool prevents the implementation of robust and generalizable post-processing methods for scar quantification, as these most often require manual segmentation of the scar/blood pool interface [6]. Application of black-blood LGE (BL-LGE) imaging to CMR has been reported in multiple studies, mostly to overcome some of the issues observed with conventional BR-LGE images [7–13]. While these studies have shown the potential of BL-LGE for challenging the longstanding dominance of BR-LGE, they have, thus far, received only limited clinical attention. Indeed, most of these sequences have been designed to exclusively acquire data during a breath-hold. Such sequences are prone to motion artifacts, particularly in cardiac protocols requiring repetitive breath-holds [14], and are not suitable for vulnerable patients with dyspnea. To this end, Kellman et al. have introduced a free-breathing strategy, based on single-shot two-dimensional (2D) BL-LGE images, non-rigid motion correction and image averaging [8]. While this technology inherits the merits of free-breathing imaging, it also comes with its set of drawbacks, including long scan times and complex parameter optimization.

The purpose of this study was to assess the clinical performance of a fast 2D BL-LGE sequence, which combines free-breathing T_1 -rho-prepared ($T_1\rho$) single-shot acquisitions with an advanced non-rigid motion-compensated patch-based reconstruction

2. Material and methods

The study was ethically approved by the institutional national French review board (ref.2018/03, Comité de Protection des Personnes, Ile de France IV, France) and conformed to the declaration of Helsinki. All patients provided informed consent for participation in this study.

2.1. Free-breathing 2D BL-LGE acquisition

Acquisitions were performed on a 1.5T clinical scanner (Magnetom Aera®, Siemens Healthcare) with a dedicated 32-element spine coil and an 18-element body coil. An electrocardiogram (ECG)-triggered 2D single-shot, balanced steady-state free-precession (bSSFP) BL-LGE sequence was implemented (Fig. 1). The sequence incorporates a non-selective inversion pulse (pulse duration = 10 msec), followed by an adiabatic $T_1\rho$ preparation module (spin-lock time [TSL] = 27 msec) to suppress the signal from both the blood and healthy myocardium [15]. This $T_1\rho$ module first plays out a 90° tip-

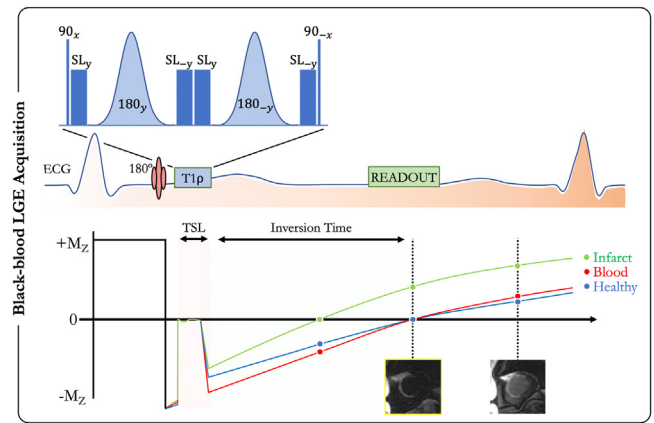


Fig. 1. Schematic overview of the proposed free-breathing single-shot 2D BL-LGE sequence. A 180 degrees inversion pulse is followed by an adiabatic $T_1\rho$ preparation module composed of four spin locks, two refocusing pulses and tip-down tip-up rectangular pulses. The spin-lock duration (TSL = 27 ms), controlling the degree of suppression of blood and viable myocardium signals, was optimized with an extended phase graph simulation framework while the inversion time is selected prior to imaging with a dedicated scout scan. Abbreviations: BL, black-blood; LGE, late gadolinium enhancement; ECG, electrocardiogram; TSL, spin-lock time; SL, spin-lock; IR, inversion recovery; M_0 , longitudinal magnetization; Acq, acquisition.

down pulse along the x-axis to rotate the magnetization, followed by four spin-lock pulses with alternating phases ($SL_{\pm y}$) and fixed duration, and two adiabatic refocusing pulses ($180_{\pm y}$) [16]. A final 90° tip-up pulse is played out to return the magnetization to the z-axis. The rotation angle of the spin-lock components was defined using the following equation $\alpha_{SL} = 2\pi \times FSL \times TSL$ where FSL (500 Hz) and TSL are the spin-lock frequency and spin-lock time, respectively. A crusher gradient is then used to remove any residual transverse magnetization. For each slice, four single-shot images were acquired sequentially in mid-diastole during 13 heartbeats (repetition time of two heartbeats to allow for full magnetization recovery). Data were acquired during free-breathing with full left ventricular coverage.

2.2. Non-rigid motion-compensated patch-based reconstruction

The proposed framework for free-breathing 2D BL-LGE consisted of three different stages: *i*), parallel imaging reconstruction of each single-shot image; *ii*), shot-to-shot non-rigid motion field estimation; and *iii*), non-rigid motion-compensated 2D patch-based reconstruction of a single high-quality BL-LGE image.

2.2.1. Shot-to-shot non-rigid motion field estimation

Single-shot images were first reconstructed using a conventional parallel imaging GRAPPA algorithm [17]. Shot-to-shot 2D non-rigid motion field estimation was subsequently performed. A regularization term that penalizes the L2-norm of motion-field gradients was employed using spline-based free-form deformation, considering the first BL-LGE shot as the reference image. The process was repeated until convergence at the finest scale, as reported by Odille et al. [18].

2.2.2. Motion-compensated patch-based reconstruction

The estimated 2D non-rigid motion fields are directly incorporated into a general matrix description (GMD) reconstruction framework [19,20]. Given that single-shot techniques sacrifice resolution and signal-to-noise ratio in favor of faster measurements, the GMD reconstruction needs to be adapted to work under the influence of noise. Patch-based reconstructions have recently attracted interest in the MR community for their ability to deal with noise and undersampling and have enabled high-resolution three-dimensional (3D) coronary MR angiography [21,22] and 3D LGE imaging [23,24]. These

techniques exploit the inherent redundancies of the heart anatomy on a local (*i.e.*, within a patch) and non-local (*i.e.*, between similar patches within a neighborhood) basis, through an efficient iterative low-rank decomposition and thresholding. The proposed framework combines GMD with a patch-based formalism for noise-less non-rigid motion-compensated BB-LGE, and can be formulated as the following augmented Lagrangian [25]:

$$\mathcal{L}_\mu(X, Z, L) = \|EX - Y\|_2^2 + \lambda \|Z\|_* + L^H(RX - Z) + \frac{\mu}{2} \|RX - Z\|_2^2 \quad (1)$$

where E is the generalized encoding operator (see Eqs. 2 and 3), X is the BB-LGE image to reconstruct and Y are the multi-coil k-spaces acquired at different respiratory states t . The patch operator R extracts similar noisy 2D patches from a reference patch and builds a self-similarity 2D matrix made by vectorizing and concatenating each of these patches [26]. A low-rank (*i.e.*, clean) representation can be extracted from this matrix by applying a singular value decomposition and by truncating the singular values below a threshold given by λ . Here, $\|\cdot\|_*$ depicts the nuclear norm, Z is the dual variable and $\mu > 0$ is the penalty parameter. The superscript H denotes the Hermitian transpose. The generalized encoding operator E and its Hermitian E^H are composed of different operators that are applied in cascade:

$$EX = \begin{bmatrix} \xi_1 \mathcal{F} \sigma_1 U_1 \\ \vdots \\ \xi_{N_{bins}} \mathcal{F} \sigma_1 U_{N_{bins}} \\ - \\ \vdots \\ - \\ \xi_1 \mathcal{F} \sigma_{N_{coils}} U_1 \\ \vdots \\ \xi_{N_{bins}} \mathcal{F} \sigma_{N_{coils}} U_{N_{bins}} \end{bmatrix} \quad \text{and} \quad E^H Y = \sum_{t=1}^{N_{bins}} U_t^H \sum_{c=1}^{N_{coils}} \sigma_c^H \mathcal{F}^H \xi_t^H Y_{t,c} \quad (2)$$

Where U_t are the estimated 2D non-rigid motion fields for shot t , σ_c the c^{th} coil sensitivity weighting operator, \mathcal{F} is the 2D Fourier transform and ξ_t the sampling matrix for shot t . Here, $N_{bins} = 4$ and N_{coils} are the number of respiratory bins and the number of coils, respectively. Solving Eq. 1 using the alternating direction method of multipliers (ADMM) consists of the iterations:

$$\begin{aligned} X^{k+1} &:= \operatorname{argmin}_X \mathcal{L}_\mu(X, Z^k, L^k) \\ &= \operatorname{argmin}_X \|EX - Y\|_2^2 + L^{kH}(RX - Z^k) + \frac{\mu}{2} \|RX - Z^k\|_2^2 \end{aligned} \quad (3)$$

$$\begin{aligned} Z^{k+1} &:= \operatorname{argmin}_Z \mathcal{L}_\mu(X^k, Z, L^k) \\ &= \operatorname{argmin}_Z \lambda \|Z\|_* + L^{kH}(RX^k - Z) + \frac{\mu}{2} \|RX^k - Z\|_2^2 \end{aligned} \quad (4)$$

$$L^{k+1} := L^k + \mu (RX^{k+1} - Z^{k+1}) \quad (5)$$

The variables X and Z are updated in an alternating fashion whereas the last equation is the ADMM dual variable update.

X Optimization (Eq. 3): This optimization is a motion-compensated reconstruction that incorporates the denoised 2D image Z^k as prior information (Tikhonov-type regularization [27]). This equation can be efficiently solved using the conjugate gradient method.

Z Optimization (Eq. 4): This optimization is a 2D patch-based denoising applied to the previously reconstructed motion-compensated 2D BB-LGE image X . This problem is formulated on a patch scale as detailed above. The denoising procedure is repeated in a sliding window fashion for all the pixels in the image and the final denoised 2D volume is obtained after aggregation. More details to solve the above equation can be found in Bustin et al [26]. Finally, the dual variable L is updated by integration of the residual between the

reconstruction motion-compensated BB-LGE image and the denoised 2D prior.

2.2.3. Reconstruction parameters

Reconstruction parameters for the proposed motion-compensated patch-based reconstruction were empirically optimized on 10 datasets (not reported here) and were kept fixed for all reconstructions. The patch size (5×5 pixels in this study) reflects the degree of structural information within each patch and the singular value truncation parameter ($\lambda = 0.1$ in this study) controls the amount of regularization. Five outer ADMM iterations were performed. The image reconstruction parameters were identical for both phantom and in vivo experiments.

2.3. Simulation study

Extended phase graph simulations [28] were first performed to analyse signal generation and evolution of the proposed sequence as a function of time. The sequence was simulated for 1.5T parameters of $T_1/T_2 = 455/190$ 548/45, 290/40 msec, corresponding to post-contrast blood, viable myocardium, and scar tissues, respectively, flip angle (FA), 60° ; TR/TE, 2.9/1.2 msec; spin-lock radiofrequency, 500 Hz; data-acquisition window, 100 msec; 2 recovery heartbeats and a simulated heart rate of 60 beats per minute. As opposed to other BL-LGE sequences [8,9], the distance between the inversion and $T_1\rho$ preparation pulses was kept constant and set to the minimal time permitted, such that only the inversion time (TI) had to be optimized. The influences of the timing parameters TI (ranging from 1 to 400 msec) and $T_1\rho$ preparation times (ranging from 1 to 200 msec) were examined for their effectiveness in suppressing both blood and myocardium signals. Simulations were performed in MATLAB (version R2019b, The MathWorks, Natick, Massachusetts, USA).

2.4. Phantom study

A moving phantom experiment was performed to assess the black-blood properties of the proposed sequence and to understand how the proposed motion-compensated sequence performs in a motion-controlled environment. The setup included both a moving phantom comprised of 12 different vials with characteristic T_1 and T_2 values [29] and a static bottle of water. To understand how the proposed motion-compensated sequence performs in a motion-controlled environment, we designed an MR-compatible setup consisting of a moving Plexiglas trolley positioned on four wheels and connected to an actuator to mimic breathing motion. The trolley consistently moved in a superior-inferior direction relative to the heart at a frequency of 15 cycles/min with a maximum amplitude of 18 mm as previously observed in adults [30]. Imaging parameters for the phantom study were: field of view (FOV), 270 mm² and simulated ECG, 60 bpm. Other relevant parameters are shown in Table 1. Three different acquisitions were performed for comparison purposes: *i*), a motion-free BL-LGE acquisition; *ii*), a motion-induced BL-LGE acquisition as described above; and *iii*), a conventional BR-LGE sequence with standard inversion recovery preparation. The TI was set to null the signal from the vial mimicking viable myocardium for the BR-LGE sequence and to null the signal from the vials simulating blood and scar tissues for the BL-LGE sequence. The $T_1\rho$ duration and frequency were set to 27 msec and 500 Hz, respectively.

All images were analyzed by drawing circular regions-of-interest (ROIs) with an area of 1.9 cm² in the phantom vials mimicking post-contrast blood, myocardium, and scar tissues. Mean signal intensity (SI) was extracted for each vial.

Table 1
Acquisition parameters for reference breath-held BR-LGE and proposed free-breathing BL-LGE sequences.

Parameter	BR-LGE	BL-LGE
Repetition time (msec)	3.9	2.9
Echo time (msec)	1.7	1.2
Flip angle (degrees)	10	60
Field of view (mm)	380 × 297	380 × 315
Fat suppression	SPIR	No
Acquired resolution (mm)	2.0 × 1.5 × 10.8	2.0 × 1.5 × 6
Reconstructed resolution (mm)	1.5 × 1.5 × 6	1.5 × 1.5 × 6
Number of slices	26 (26, 26)	14 (14, 16)
Phase oversampling (%)	15	0
Slice oversampling (%)	0	N.A.
Asymmetric echo	Yes	Yes
Acquisition window (msec)	236	160
Inversion time (msec)	260 (240, 270)	100 (79, 120)
T _{1ρ} duration (msec)	N.A.	27
T _{1ρ} frequency (Hz)	N.A.	500
Scan acceleration	GRAPPA x2	GRAPPA x2
Trigger pulse* (RR interval)	1	2
Bandwidth (Hz/pixel)	360	849
Breath-hold	Yes	No
Sequence	3D GRE	2D bSSFP

Quantitative variables are expressed as medians followed by interquartile ranges in parentheses.

BR: Bright-blood; BL: Black-blood; LGE: Late gadolinium enhancement. N.A.: Not applicable.

* Data acquisition every second (standard) or every third R-R interval.

2.4. Patient study

2.4.1. CMR protocol acquisition

A prospective patient study was conducted in 51 consecutive patients who were referred between October 2020 and January 2021 to undergo clinical CMR for known or suspected heart disease (Fig. 2). The exclusion criteria were any contraindications to CMR. Acquisitions were performed with the same 1.5T clinical scanner (Magnetom Aera®, Siemens Healthcare) than the one used for the phantom study. Breath-held BR-LGE and proposed free-breathing BL-LGE images were acquired in random order 12 min after the intravenous injection of 0.2 mmol/kg gadoterate meglumine (Dotarem®, Guerbet). Sequence parameters are provided in Table 1. An additional dedicated TI scout scan was performed prior to BL-LGE imaging. The scout images could be visualized in real time and the TI scout sequence was halted when both blood and healthy myocardium were nulled, resulting in less than 15 sec processing time (Fig. 3). Acquisition and reconstruction times for BL-LGE imaging were recorded.

2.4.2. CMR image analysis and interpretation

Image entropy and normalized gradient squares (NGS) were used to quantify signal dispersion and image sharpness, respectively [31]. These two metrics were computed on the non-corrected and motion-corrected BL-LGE images in a rectangular ROI encompassing the heart. For each LGE dataset, the scar-to-myocardium, scar-to-blood, and blood-to-myocardium relative contrasts were extracted in a slice with the most notable scar. The relative contrast of tissue S₁ to tissue S₂ was calculated as the difference in signal intensity, measured in ROIs, between S₁ and S₂ divided by the mean signal intensity in S₂. Regions of interest were manually drawn using MATLAB (version R2019b, The MathWorks).

2.4.3. Clinical value of BL-LGE

Two experienced radiologists (H.C. and S.S.), 18 and 5 years' experience in CMR, respectively) reviewed the BR-LGE and BL-LGE images in consensus. Images were analyzed in a random order using CVI42 (Circle Cardiovascular Imaging, Calgary, Canada), with two reading sessions being organized one month apart to ensure independent interpretation of BR-LGE and BL-LGE images. Contrast scaling and magnification could be adjusted by the readers for each sequence. Image quality was graded in consensus using a 4-point scale (1-non-diagnostic with severe artifacts, 2-less than adequate, 3-adequate with moderate artifacts, 4-diagnostic image quality). Reasons for image quality scores other than 4 were reported. The extent of LGE was quantified in each of the 17-segments of the AHA model [32]. For each dataset, LGE findings were categorized as absent with confidence, present with confidence or inconclusive. The distribution of LGE was described as primarily midwall, subepicardial or subendocardial. LGE patterns involving the papillary muscles and the right ventricular insertion points on the septum were also recorded.

2.5. Statistical analysis

Statistical analyses were performed using SPSS Statistics version 27 (IBM). Quantitative variables were expressed as means, standard deviations (SD) and ranges or medians, interquartile ranges (IQR; Q1, Q3) and ranges. Shapiro-Wilk test of normality was employed to check that continuous variables had a normal distribution. Dependent continuous variables were compared using paired-sample *t*-test or Wilcoxon signed rank test, depending on data normality. Dependent categorical variables were compared using the paired-sample McNemar test. The Pearson correlation coefficient was calculated to determine the correlation between image quality and heart rate. All statistical tests were two-sided and values of *P*<0.05 indicated statistical significance.

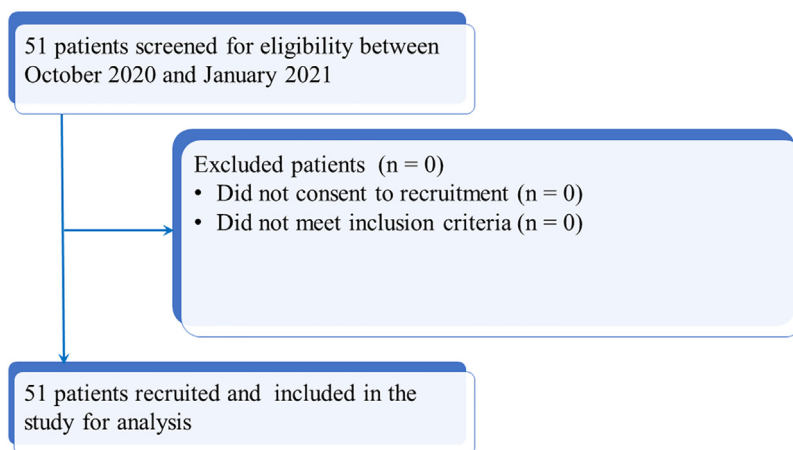


Fig. 2. Study flowchart outlines the selection and analysis of participants with known or suspected heart disease.

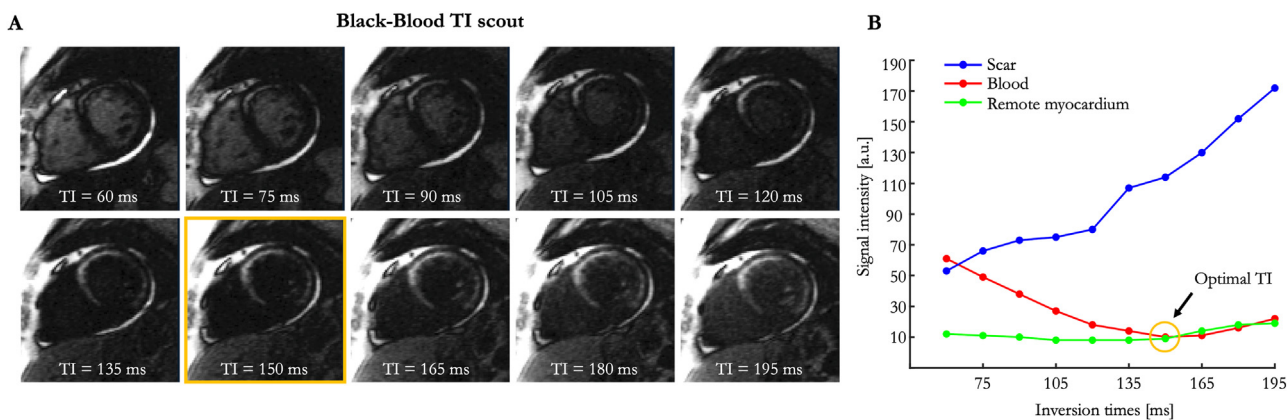


Fig. 3. Proposed black-blood TI scout images in a patient with myocardial infarction. (A) TI scout images are visualized in real-time and the sequence is halted when the optimal TI image (here at TI = 150 msec) is seen. (B) Signal evolutions of blood, viable myocardium and scar tissues on the TI scout images. Abbreviation: TI, inversion time.

3. Results

3.1. Simulation and phantom studies

Simulations showed that the combination of an inversion pulse with a $T_{1\rho}$ preparation module allows for near-complete nulling of

both viable myocardium and blood signals, with zero planes intersecting at a $T_{1\rho}$ duration of 27 msec (Fig. 4). At this point, viable myocardium and blood signals are nulled whereas scar signal remains positive. This value was thus used in the following imaging experiments. Phantom images reconstructed without motion correction exhibited typical ghosting artifacts that were consistently removed

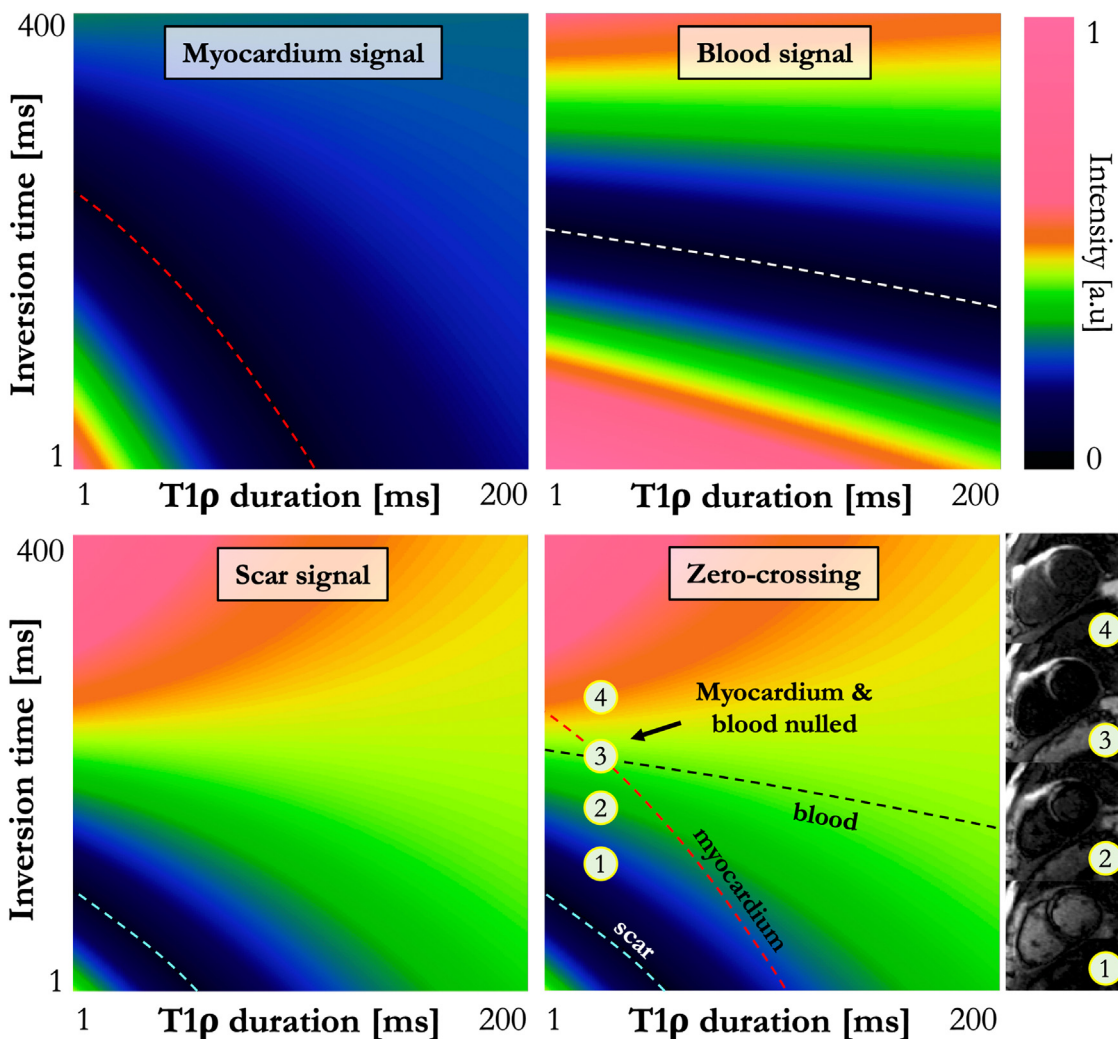


Fig. 4. The performance of the proposed black-blood sequence is illustrated through extended phase graph simulations, which display the signal evolution (normalized longitudinal magnetization M_z) of blood ($T_1/T_2 = 455/190$ msec), viable myocardium ($T_1/T_2 = 548/45$ msec) and scar ($T_1/T_2 = 290/40$ msec) tissues when varying the inversion time and the duration of the $T_{1\rho}$ cluster (TSL). A near-complete nulling of both blood and viable myocardium signals is obtained for a $T_{1\rho}$ duration of 27 msec. At this intersection point, both blood and viable myocardium are nulled whereas scar signal remains positive.

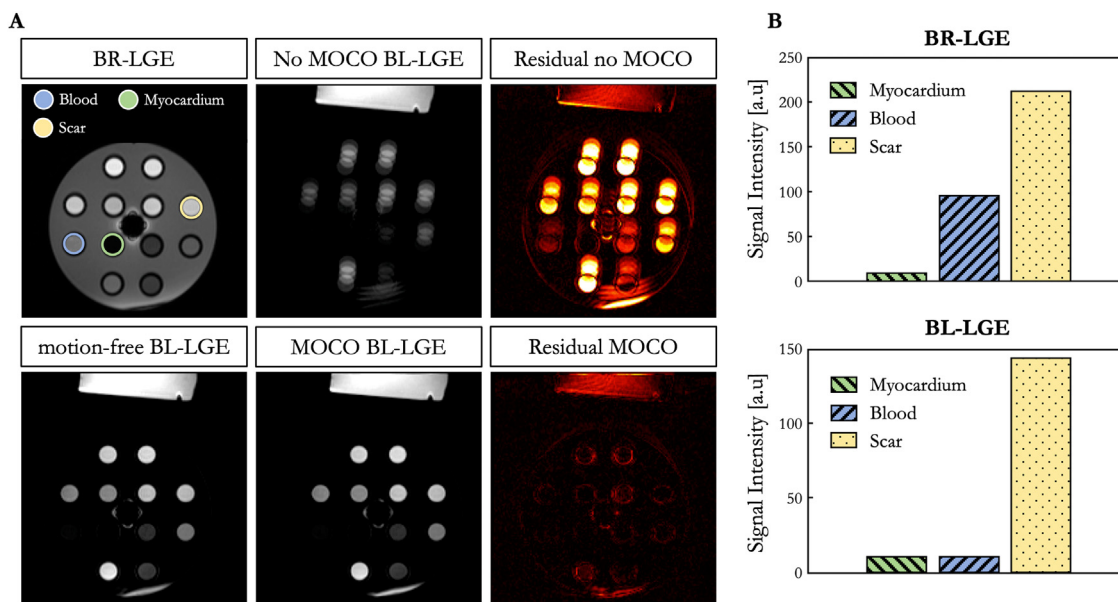


Fig. 5. Impact of non-rigid motion correction in a setup including a static (bottle of water) and moving T_1/T_2 phantom (A) and measured signal intensities in vials with T_1/T_2 corresponding to post-contrast blood, viable myocardium and scar tissues (B). Ghosting artifacts are visible on the non-corrected BL-LGE image and corresponding residual image. The non-rigid motion-corrected BL-LGE image is free of any motion artifacts while maintaining the desired black-blood and black-myocardium contrasts (A). The BL-LGE image shows clear signal suppression of both blood and viable myocardium compartments with high scar-to-myocardium and scar-to-blood contrasts (B). Conventional BR-LGE imaging effectively suppresses the signal from the viable myocardium compartment but does not suppress the blood signal. Abbreviations: BR, bright-blood; BL, black-blood; LGE, late gadolinium enhancement; MOCO, motion-correction.

with the proposed motion-compensated patch-based reconstruction (Fig. 5). Signals extracted from vials corresponding to viable myocardium, blood and scar tissues are shown in Fig. 5b for both conventional BR-LGE and proposed motion-corrected BL-LGE sequences. As expected, viable myocardium signal was properly cancelled ($SI_{bright}^{scar} / SI_{bright}^{myo} = 23.7$), on the BR-LGE sequence, whereas blood signal remained positive ($SI_{bright}^{scar} / SI_{bright}^{blood} = 2.2$). Conversely, the proposed black-blood sequence effectively nulled both the blood ($SI_{black}^{scar} / SI_{black}^{blood} = 14.4$) and viable myocardium ($SI_{black}^{scar} / SI_{black}^{myo} = 14.4$) signals and allows the scar tissue to appear bright on the images.

3.2. Patient study

3.2.1. Patients characteristics

Fifty-one participants were recruited. There were 37 men and 14 women with a mean age of 55 ± 15 (SD) years (range: 19–81 years) and a median left ventricular ejection fraction of 43% (IQR: 35, 58). Baseline characteristics of the patient cohort are shown in Table 2. Clinical indications for CMR were: (i), the follow-up and/or prognostic assessment of a known structural heart disease in 32/51 patients (29 with ischemic cardiomyopathy and three with dilated cardiomyopathy, all diagnoses being confirmed on CMR); (ii), the etiological diagnosis of a suspected cardiomyopathy in 11/51 patients (the final CMR diagnosis being dilated cardiomyopathy in two, ischemic cardiomyopathy in four, hypertrophic cardiomyopathy in two, and negative CMR in three); or (iii), the etiological diagnosis of an acute coronary syndrome in 8/51 patients (the final CMR diagnosis being acute myocardial infarction in one patient, acute myocarditis in two, acute pericarditis in one, and negative CMR in four). Complete 2D BL-LGE datasets were successfully acquired in all patients. Mean acquisition time with the proposed free-breathing BL-LGE sequence was 115 ± 25 (SD) sec (range: 64–160 sec). Reconstruction time on the scanner was 3 sec per slice.

3.2.2. Motion correction quality

The mean respiratory excursion of the heart between the four single-shot repetitions in vivo was 12 ± 7 (SD) mm (range: 7–22 mm).

The use of non-rigid motion correction efficiently corrected for this motion (Fig. 6), with significantly higher NGS scores after motion correction (mean difference: 2.8; 95% confidence interval [CI]: 2.1, 3.6) ($P < 0.01$). Image entropy was significantly lower after motion correction (mean difference: -0.04; 95% CI: -0.05, -0.03) ($P < 0.01$).

3.2.3. Image quality

Image quality differed significantly between BR-LGE and BL-LGE images ($P < 0.01$) (Table 3). As graded by the two experts, it was diagnostic for 34/51 (67%) of the reference BR-LGE images, and 44/51

Table 2
Baseline characteristics of 51 participants.

Patient characteristics	
Male	37 (73)
Age (year)	55 ± 15 [19–81]
Heart rate (beats/min)	67 (55, 74)
Weight (kg)	78 ± 20 [40–165]
Height (cm)	173 (166, 180)
Body mass index (kg/m ²)	27 ± 7 [11–64]
CMR diagnosis	
Ischemic cardiomyopathy	34 (67)
Dilated cardiomyopathy	5 (10)
Hypertrophic cardiomyopathy	2 (4)
Myocarditis	2 (4)
Pericarditis	1 (2)
Negative CMR	7 (14)
Cardiac function	
LVEF (%)	43 (35, 58)
Reduced LVEF	33 (65)
LV EDV / BSA (mL/m ²)	104 (87, 129)
LV ESV / BSA (mL/m ²)	57 (40, 84)

Values are n (%), median (interquartile range) or mean \pm standard deviation followed by ranges in brackets
CMR, Cardiovascular magnetic resonance; LVEF, Left ventricular ejection fraction; EDV, End-diastolic volume; BSA, Body surface area; ESV, End-systolic volume; LGE, Late gadolinium enhancement.

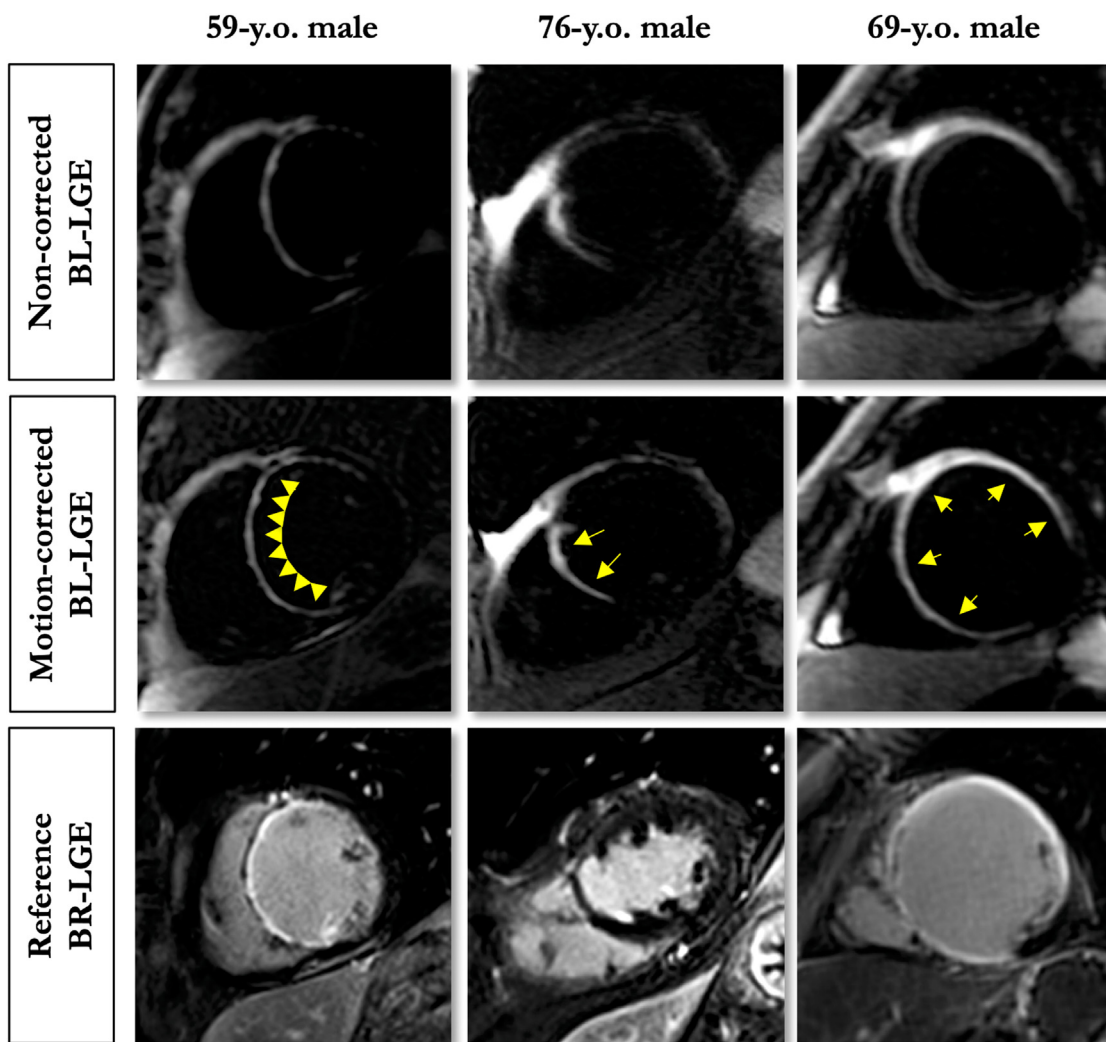


Fig. 6. Impact of non-rigid motion correction on myocardial scar visualization in free-breathing BL-LGE imaging. Improved overall image quality, image sharpness and visualization of LGE lesions are obtained when correcting for respiratory-induced non-rigid motion of the heart (middle row) compared with the non-corrected BL-LGE images (top) in these three patients. After motion correction, a good correspondence of LGE lesions can be observed between the proposed free-breathing BL-LGE imaging sequence and the reference clinical breath-held BR-LGE sequence. Abbreviations: BR, bright-blood; BL, black-blood; LGE, late gadolinium enhancement.

Table 3
Late gadolinium enhancement findings, relative contrast, and image quality in 51 patients.

	Reference BR-LGE imaging only	Proposed BL-LGE imaging only	P value
LGE characteristics			
LGE extent (number of segments) ^a	4 (1, 6)	5 (2, 7)	<0.01
Negative myocardial LGE	5 (10)	9 (18)	0.13
Positive myocardial LGE	38 (75)	42 (82)	0.06
Inconclusive myocardial LGE	8 (16)	0 (0)	<0.01
Relative contrast and image quality			
Scar-to-myocardium	4.0 ± 3.7 [0.5–17.0]	8.1 ± 4.4 [2.3–18.0]	<0.01
Scar-to-blood	0.4 ± 0.6 [-0.2–2.1]	7.6 ± 4.9 [2.3–20.0]	<0.01
Blood-to-myocardium	2.5 ± 1.8 [-0.5–7.8]	0.2 ± 0.4 [-0.5–1.0]	<0.01
Image quality	3.6 ± 0.7 [2–4]	3.9 ± 0.2 [3–4]	<0.01

Values are n (%), median (interquartile range[Q1, Q3]) or mean ± standard deviation (range). BR, Bright-blood; BL, Black-blood; LGE, Late gadolinium enhancement; Bold indicates significant P value.

^a refers to patients with positive LGE.

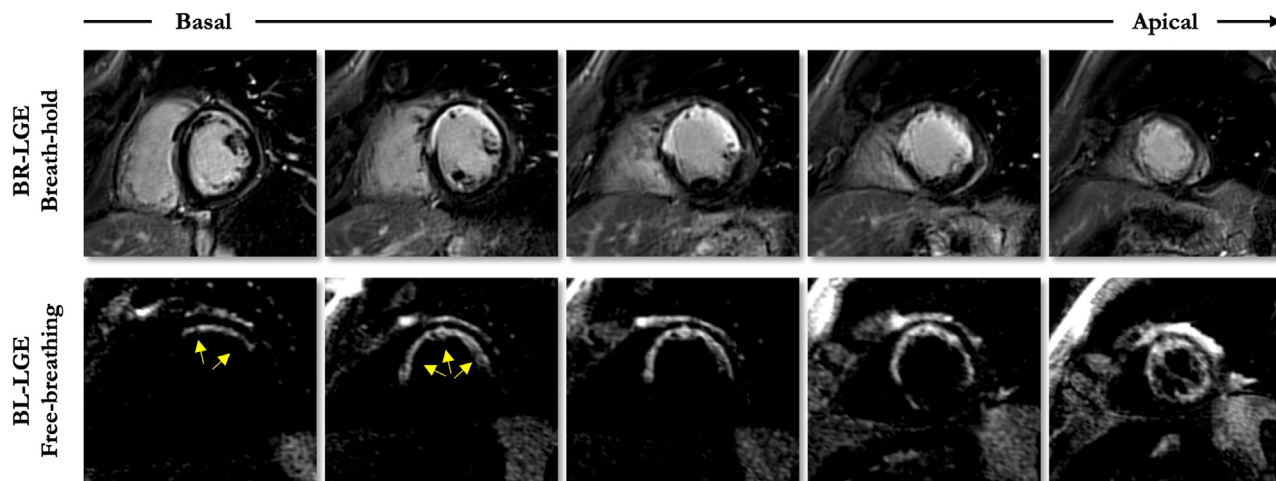


Fig. 7. Comparison between the reference breath-held BR-LGE (top) and the proposed motion-compensated free-breathing BL-LGE (bottom) images in a 43-year-old male patient with myocardial infarction in the left anterior descending artery territory. Motion-corrected BL-LGE clearly identifies areas of enhancement, particularly at the apical level, whereas the poor blood-scar contrast on the reference BR-LGE images makes scar visualization more difficult. Abbreviations: BR, bright-blood; BL, black-blood; LGE, late gadolinium enhancement.

(86%) of the BL-LGE images (Figs. 7 and 8). No dataset was scored nondiagnostic in either LGE sequences. A poor correlation between impaired image quality on BL-LGE images and heart rate was found ($r = 0.35$). Impaired image quality (Table 4) in the breath-held BR-LGE datasets was attributed to residual motion artefacts (10/51 vs. 1/51 for BL-LGE) and to suboptimal TI selection (6/51 vs. 4/51).

3.2.4. Relative contrast

Compared with the reference BR-LGE images, the average scar-to-myocardium relative contrast in the BL-LGE images significantly increased by 102.5% to 8.1 ± 4.4 (SD) (range: 2.3–18.0) ($P < 0.01$).

Similarly, a significant increase in scar-to-blood relative contrast (0.4 ± 0.6 [SD] [range: -0.2–2.1] vs. 7.6 ± 4.9 [SD] [range: 2.3–20.0]) ($P < 0.01$) was observed. Owing to the nulling of both blood and viable myocardium signal, a significant decrease in blood-to-myocardium relative contrast (2.5 ± 1.8 [SD] [range: -0.5–7.8] vs. 0.2 ± 0.4 [SD] [range: -0.5–1.0]) ($P < 0.01$) was observed with the proposed sequence (Table 3).

3.2.5. LGE analysis at the segmental level

A total of 867 myocardial segments were analyzed on both sequences. All 207 segments with positive LGE on BR-LGE images

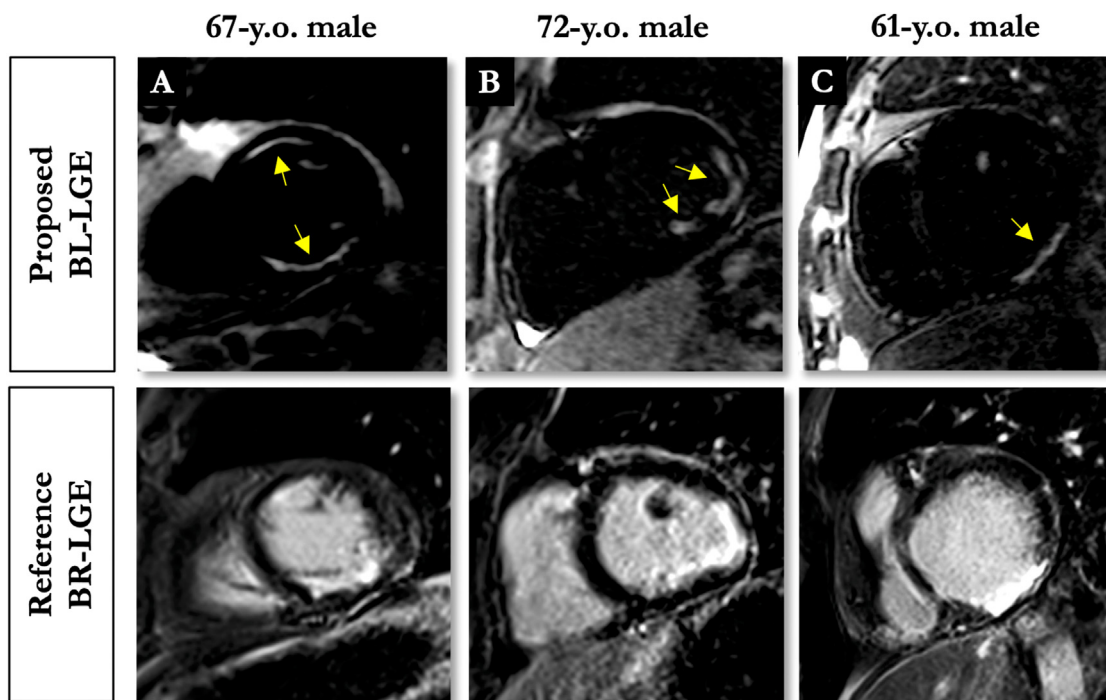


Fig. 8. Proposed free-breathing motion-compensated BL-LGE (top) and reference breath-held BR-LGE (bottom) images in three patients with evidence of myocardial injuries. (A) 67-year-old male with subendocardial infarctions in the right coronary artery and first diagonal territories. (B) Late enhancement in a 72-year-old man with subendocardial myocardial infarction involving five segments in the left circumflex artery territory. (C) 61-year-old male showing transmural late enhancement in the infero- and infero-lateral segments. Abbreviations: BR, bright-blood; BL, black-blood; LGE, late gadolinium enhancement.

Table 4
Overview of the reasons for impaired image quality (scores other than 4) on reference BR-LGE and proposed BL-LGE images.

Reason for impaired image quality	Reference BR-LGE (n = 51)	Proposed BL-LGE (n = 51)
Folding artifacts	1	2
Motion / blurring	10	1
Suboptimal contrast	6	4
Total	17	7

Note: Image quality was deemed impaired when score was graded other than 4. BR, bright-blood; BL, black-blood; LGE, late gadolinium enhancement.

were also positive on BL-LGE. BL-LGE detected additional hyper-enhanced segments in 18/51 (35%) patients. Overall, BL-LGE imaging detected 33 additional segments (16% more than on BR-LGE), resulting in a larger extent of LGE on BL-LGE (median, 5 segments [IQR: 2, 7 segments] vs. median, 4 segments [IQR: 1, 6 segments] ($P < 0.01$). These 33 additional LGE segments observed on BL-LGE only were subendocardial in 25/33, subepicardial in 2/33, and midwall in 6/33. Of note, these involved papillary muscles in 8/33 segments (24%), and the inferior right ventricular insertion point in 3/33 (9%).

3.2.6. LGE analysis at the patient level

Myocardial LGE was identified with confidence in 38 patients (75%) on BR-LGE and in 42 patients (82%) on BL-LGE ($P = 0.06$) (Table 3). All patients showing myocardial LGE on BR-LGE were also positive on BL-LGE. Overall, the interpretation of myocardial injuries derived from BL-LGE imaging was modified in 8/51 (16%) patients (Fig. 9). In 4/51 (8%) patients, LGE was positive with confidence on BL-LGE imaging whereas conventional BR-LGE imaging remained inconclusive. The LGE pattern in these patients was sub-epicardial in 1/4, subendocardial in 2/4, and midwall on right ventricular inferior insertion point in 1/4. Similarly, BL-LGE imaging could rule out areas of hyperenhancement in 4/51 (8%) patients with confidence while BR-LGE imaging was inconclusive. In all of these patients, BR-LGE showed concealed enhancements near the endocardium of the left ventricular free wall and/or papillary muscles, whose myocardial

location remained unclear. These were non-visible on BL-LGE, thus likely related to contrast trapping in the blood pool adjacent to the endocardium. In terms of diagnosis, the use of BL-LGE imaging could reveal myocardial infarction in 2/51 (4%) and myocarditis in 1/51 (2%) and support the diagnosis of hypertrophic cardiomyopathy in 1/51 (2%). Furthermore, BL-LGE imaging could rule out the diagnosis of myocardial infarction in 4/51 (8%). Final CMR diagnoses using both BR-LGE and BL-LGE were ischemic cardiomyopathy in 34/51 (67%), dilated cardiomyopathy in 5/51 (10%), hypertrophic cardiomyopathy in 2/51 (4%), myocarditis in 2/51 (4%), pericarditis in 1/51 (2%) and negative CMR in 7/51 (14%).

4. Discussion

Accurate identification of myocardial injury using non-invasive BR-LGE CMR has critical diagnostic and prognostic value in a wide range of cardiomyopathies and has immediate impact on therapy. In the context of ischemic heart disease, however, this task can be particularly challenging. The presence of subendocardial LGE foci which are, by definition, located at the interface blood-myocardium can make BR-LGE images difficult to interpret due to poor contrast between blood pool and scar tissue. For that reason, accurate assessment of myocardial scar location, transmuralty and size with established BR-LGE sequences is labor intensive and requires experience and clinical expertise. The proposed free-breathing 2D BL-LGE framework, as an adjunct to BR-LGE, appears to effectively overcome this limitation. The present approach illustrates the applicability in a routine clinical workflow of a free-breathing motion-corrected BL-LGE imaging technique that does not require complex training and scanner adjustments while acquiring and reconstructing images in a fast (2 min scan time) and efficient (inline processing) manner.

In the context of dark-blood LGE imaging, flow-independent techniques, exploiting preparation pulses, have proved useful in uncovering scar patterns that may be otherwise confused with blood signal, and have provided the cornerstone of a series of 2D and 3D studies [8,9]. In particular, the use of T2-prepared pulses combined with inversion recovery has offered means for signal modulation that helps darken the blood signal and null the healthy myocardium

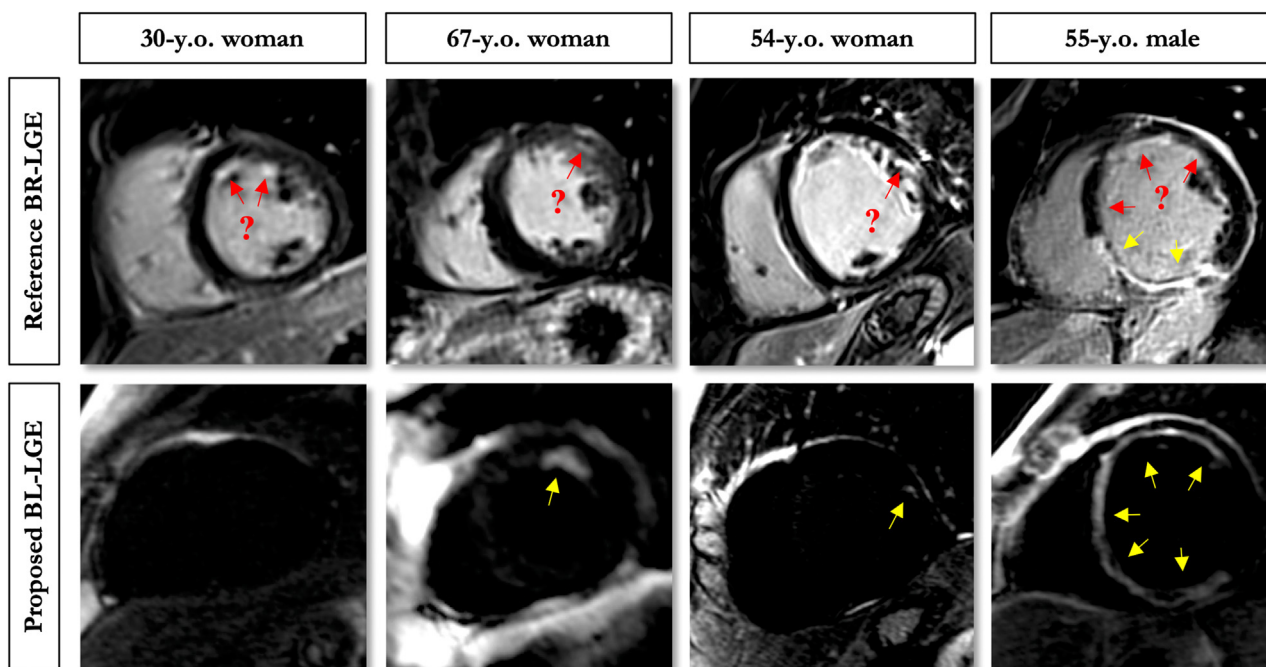


Fig. 9. Examples of BL-LGE images obtained in four patients where the presence of LGE was inconclusive on BR-LGE imaging. LGE patterns could easily be observed (yellow arrows) or ruled out (first patient) with the proposed motion-corrected BL-LGE images. Abbreviations: BR, bright-blood; BL, black-blood; LGE, late gadolinium enhancement.

tissue [8,10]. Alternative approaches involving magnetization transfer pulses, so-called FIDDLE [11] or TRAMINER [12,13], have also been proposed.

Until now, one main strategy has been proposed to overcome the problem of motion in free-breathing 2D BL-LGE imaging [8]. The suggested single-shot T_2 -prepared inversion recovery sequence acquires multiple single-shot images that are then co-registered and averaged. While this technology inherits the merits of free-breathing imaging, it also comes with drawbacks. Firstly, signal-to-noise ratio has to be traded for long scan times (about 5 min to acquire 9 slices). Without a strategy to handle varying TIs throughout the acquisition, a long time interval between the first and last slices acquired may also compromise the homogeneity of blood and myocardium signal suppression. Secondly, the contrasts between blood, viable myocardium and scar depend on two parameters that need to be carefully chosen by the technician. Although requiring little time, this step however adds complexity, necessitate additional technician training, and increase the operator dependency as much as time to the clinical workflow.

The clinical performance of the proposed free-breathing BL-LGE approach was demonstrated against reference breath-held BR-LGE in a real clinical situation. We found significantly higher image quality on the BL-LGE images than on the BR-LGE images. Degradation of image quality in breath-held BR-LGE was most often attributed to remaining blurring and motion artifacts that could be related to the often long and repetitive breath-holds. Owing to its free-breathing acquisition, the BL-LGE images did not suffer from motion artifacts (1/51 patients), but mostly from suboptimal TI selection (4/51 patients).

Our results indicate that BL-LGE is more sensitive in detecting myocardial injuries as compared to the conventional BR-LGE method. As expected, most of the LGE-positive lesions unravelled by BL-LGE were subendocardial scars (25/33) and/or scars involving the papillary muscles (8/33), which outlines that the increased sensitivity is a direct consequence of the blood signal cancellation. The ability of BL-LGE to detect concealed myocardial injuries would be extremely valuable to assist the etiological diagnosis of structural heart disease or to identify the cause of acute coronary syndromes with non-obstructed coronary arteries, as small subendocardial scars are quite frequent in these clinical scenarios [33].

Besides scar detection, our results also indicate that BL-LGE allows for a more thorough assessment of scar extent. This may have major implications for the primary prevention of sudden cardiac death in structural heart disease, as scar burden was shown to be a major predictor of ventricular arrhythmia events in ischemic, dilated and hypertrophic cardiomyopathies [34]. In that prospect, the present study demonstrates high contrasts between both scar and blood pool and scar and remote myocardium, which may be ideally suited to the implementation of fully automated scar segmentation approaches, thereby increasing the robustness of CMR-derived prognosis. Lastly, BL-LGE imaging may also improve the specificity of CMR in the assessment of myocardial scar and make LGE CMR interpretation less dependent on reader's expertise. This is particularly critical in case of false positive enhancement on BR-LGE images due to contrast trapping in the blood pool adjacent to the endocardium or in the vicinity of papillary muscles. In the present study, such inconclusive findings on BL-LGE imaging could be effectively ruled out in 4 patients.

The efficacy of decreasing the signal from the viable myocardium and the left ventricular blood has been previously reported for 2D breath-held [10,11,13,35,36] and 3D respiratory-navigated applications [9,37]. Among the above-mentioned strategies, FIDDLE (flow-independent dark-blood delayed enhancement), exploiting magnetization transfer preparations, has been successfully applied to small cohorts of patients at 3T and under breath-holds [11,36]. At high field strengths, magnetization transfer pulses may be preferred over $T_1\rho$ pulses as magnetization transfer increases with higher T_1 while

radiofrequency energy deposition and associated specific absorption rate are less of a concern than with $T_1\rho$ pulses. For lower field strengths, however, the use of adiabatic $T_1\rho$ pulses, as proposed in the present study, can generate contrast with relatively low sensitivity to field inhomogeneity while requiring less parameter optimization. Nevertheless, our motion-compensated approach is not limited to the proposed $T_1\rho$ -prepared sequence and could be applied to other single-shot-based techniques.

One inherent limitation is that the proposed non-rigid motion-compensated framework cannot account for through-plane motion but only residual in-plane respiratory motion. A natural mechanism for prospective through-plane motion correction would be to perform 3D acquisitions. A last set of limitations is related to the lack of anatomical information due to the equal suppression of both blood and healthy myocardium signals. Innovations aimed at joint bright- and black-blood imaging should improve spatial localization of myocardial injuries. Finally, intra-reader and inter-reader agreements in LGE analysis will be investigated in future work.

In conclusion, the proposed free-breathing motion-compensated $T_1\rho$ -prepared BL-LGE sequence can be a useful adjunct to conventional BR-LGE imaging, particularly in patients with subendocardial myocardial infarction where conventional imaging techniques suffer from poor-scar contrast. Extension of the proposed framework to 3D BL-LGE imaging is warranted.

Human rights

The study was conducted in accordance with the Declaration of Helsinki (as revised in 2013). The study was approved by the Biomedical Research Ethics Committee and all patients provided informed consent for participation in this study.

Author contributions

All authors attest that they meet the current International Committee of Medical Journal Editors (ICMJE) criteria for Authorship.

Informed consent and patient details

The authors declare that this report does not contain any personal information that could lead to the identification.

Funding

This research received specific grants from Agence Nationale de la Recherche (Award Number: Equipex MUSIC ANR-11-EQPX-0030; Recipient: Pierre Jaïs) Programme d'Investissements d'Avenir (Award Number: ANR-10-IAHU04-LIRYC) 2020 European Research Council (Award Number: ERC n715093; Recipient: Hubert Cochet). Agence Nationale de la Recherche (Award Number: ANR-21-CE17-0034-01; Recipient: Aurélien Bustin).

Ethical statement

The study was approved by the Biomedical Research Ethics Committee and all patients provided informed consent for participation in this study.

CRediT authorship contribution statement

Soumaya Sridi: Conceptualization, Methodology, Software, Validation, Formal analysis, Data curation, Writing – review & editing. **Marta Nuñez-García:** Conceptualization, Data curation, Writing – original draft. **Maxime Sermesant:** Conceptualization, Data curation, Writing – original draft. **Aurélien Maillot:** Conceptualization, Data curation, Writing – original draft. **Dounia El Hamrani:**

Conceptualization, Data curation, Writing – original draft. **Julie Magat**: Conceptualization, Data curation, Writing – original draft. **Jérôme Naulin**: Conceptualization, Data curation, Writing – original draft. **François Laurent**: Conceptualization, Data curation, Writing – original draft. **Michel Montaudon**: Conceptualization, Data curation, Writing – original draft. **Pierre Jais**: Conceptualization, Data curation, Writing – original draft. **Matthias Stuber**: Conceptualization, Methodology, Software, Validation, Formal analysis, Data curation, Writing – review & editing. **Hubert Cochet**: Conceptualization, Methodology, Software, Validation, Formal analysis, Data curation, Writing – review & editing. **Aurélien Bustin**: Conceptualization, Methodology, Software, Validation, Formal analysis, Data curation, Writing – review & editing.

References

- Patel AR, Kramer CM. Role of cardiac magnetic resonance in the diagnosis and prognosis of nonischemic cardiomyopathy. *JACC Cardiovasc Imaging* 2017;10:1180–93.
- Foussier C, Barral PA, Jerosh-Herold M, Gariboldi V, Rapacchi S, Gallon A, et al. Quantification of diffuse myocardial fibrosis using CMR extracellular volume fraction and serum biomarkers of collagen turnover with histologic quantification as standard of reference. *Diagn Interv Imaging* 2021;102:163–9.
- Longère B, Chavent MH, Coisne A, Gkizas C, Pagniez J, Simeone A, et al. Single breath-hold compressed sensing real-time cine imaging to assess left ventricular motion in myocardial infarction. *Diagn Interv Imaging* 2021;102:297–303.
- Kim RJ, Fieno DS, Parrish TB, Harris K, Chen EL, Simonetti O, et al. Relationship of MRI delayed contrast enhancement to irreversible injury, infarct age, and contractile function. *Circulation* 1999;100:1992–2002.
- Farrelly C, Rehwald W, Salerno M, Davarpanah A, Keeling AN, Jacobson JT, et al. Improved detection of subendocardial hyperenhancement in myocardial infarction using dark blood-pool delayed enhancement MRI. *Am J Roentgenol* 2011;196:339–48.
- Flett AS, Hasleton J, Cook C, Hausenloy D, Quarta G, Ariti C, et al. Evaluation of techniques for the quantification of myocardial scar of differing etiology using cardiac magnetic resonance. *JACC Cardiovasc Imaging* 2011;4:150–6.
- Henningsson M, Malik S, Botnar R, Castellanos D, Hussain T, Leiner T. Black-blood contrast in cardiovascular MRI. *J Magn Reson Imaging* 2020;1–20.
- Kellman P, Xue H, Olivieri LJ, Cross RR, Grant EK, Fontana M, et al. Dark blood late enhancement imaging. *J Cardiovasc Magn Reson* 2016;18:1–11.
- Fahmy AS, Neisius U, Tsao CW, Berg S, Goddu E, Pierce P, et al. Gray blood late gadolinium enhancement cardiovascular magnetic resonance for improved detection of myocardial scar. *J Cardiovasc Magn Reson* 2018;20:1–11.
- Francis R, Kellman P, Kotecha T, Baggiano A, Norrington K, Martinez-Naharro A, et al. Prospective comparison of novel dark blood late gadolinium enhancement with conventional bright blood imaging for the detection of scar. *J Cardiovasc Magn Reson* 2017;19:1–12.
- Kim HW, Rehwald WG, Jenista ER, Wendell DC, Filev P, van Assche L, et al. Dark-blood delayed enhancement cardiac magnetic resonance of myocardial infarction. *JACC Cardiovasc Imaging* 2018;11:1758–69.
- Muscogiuri G, Rehwald WG, Schoepf UJ, Suranyi P, Litwin SE, De Cecco CN, et al. T (Rho) and magnetization transfer and INvErSion recovery (TRAMINER)-prepared imaging: A novel contrast-enhanced flow-independent dark-blood technique for the evaluation of myocardial late gadolinium enhancement in patients with myocardial infarction. *J Magn Reson Imaging* 2017;45:1429–37.
- Song L, Ma X, Zhao X, Zhao L, DeLano M, Fan Y, et al. Validation of black blood late gadolinium enhancement (LGE) for evaluation of myocardial infarction in patients with or without pathological Q-wave on electrocardiogram (ECG). *Cardiovasc Diagn Ther* 2020;10:124–34.
- Scott AD, Keegan J, Firmin DN. Motion in cardiovascular MR imaging. *Radiology* 2009;250:331–51.
- Qi H, Bustin A, Kuestner T, Hajhosseiny R, Cruz G, Kunze K, et al. Respiratory motion-compensated high-resolution 3D whole-heart T1 ρ mapping. *J Cardiovasc Magn Reson* 2020;22:1–13.
- Nezafat R, Stuber M, Ouwkerk R, Gharib AM, Desai MY, Pettigrew RI. B1-insensitive T2 preparation for improved coronary magnetic resonance angiography at 3T. *Magn Reson Med* 2006;55:858–64.
- Griswold MA, Jakob PM, Heidemann RM, Nittka M, Jellus V, Wang J, et al. Generalized autocalibrating partially parallel acquisitions (GRAPPA). *Magn Reson Med* 2002;47:1202–10.
- Odille F, Steeden JA, Muthurangu V, Atkinson D. Automatic segmentation propagation of the aorta in real-time phase contrast MRI using nonrigid registration. *J Magn Reson Imaging* 2011;33:232–8.
- Batchelor PG, Atkinson D, Irrazaval P, Hill DLG, Hajnal J, Larkman D. Matrix description of general motion correction applied to multishot images. *Magn Reson Med* 2005;54:1273–80.
- Odille F, Vuissoz PA, Felblinger J, Atkinson D. Generalized reconstruction by inversion of coupled systems (GRICS) applied to parallel MRI. *Magn Reson Med* 2008;60:146–57.
- Bustin A, Rashid I, Cruz G, Hajhosseiny R, Correia T, Neji R, et al. 3D whole-heart isotropic sub-millimeter resolution coronary magnetic resonance angiography with non-rigid motion-compensated PROST. *J Cardiovasc Magn Reson* 2020;22:1–16.
- Akçakaya M, Basha TA, Goddu B, Goepfert LA, Kissinger KV, Tarokh V, et al. Low-dimensional-structure self-learning and thresholding: regularization beyond compressed sensing for MRI Reconstruction. *Magn Reson Med* 2011;66:756–67.
- Basha TA, Akçakaya M, Liew C, Tsao CW, Delling FN, Addae G, et al. Clinical performance of high-resolution late gadolinium enhancement imaging with compressed sensing. *J Magn Reson Imaging* 2017;46:1829–38.
- Munoz C, Bustin A, Neji R, Kunze KP, Forman C, Schmidt M, et al. Motion-corrected 3D whole-heart water-fat high-resolution late gadolinium enhancement cardiovascular magnetic resonance imaging. *J Cardiovasc Magn Reson* 2020;22:1–13.
- Boyd S, Parikh N, Chu E, Peleato B, Eckstein J, EChu BP, et al. Distributed optimization and statistical learning via the alternating direction method of multipliers. *Found Trends[®] Mach Learn* 2010;3:1–122.
- Bustin A, Ginami G, Cruz G, Correia T, Ismail TF, Rashid I, et al. Five-minute whole-heart coronary MRA with sub-millimeter isotropic resolution, 100% respiratory scan efficiency, and 3D-PROST reconstruction. *Magn Reson Med* 2019;81:102–15.
- Ying L, Xu D, Liang ZP. On Tikhonov regularization for image reconstruction in parallel MRI. *Ann. Int. Conf. IEEE Eng. Med. Biol. - Proc.*; 2004.
- Weigel M. Extended phase graphs: dephasing, RF pulses, and echoes - Pure and simple. *J Magn Reson Imaging* 2015;41:266–95.
- Lerski RA, de Certaines II. JD. Performance assessment and quality control in MRI by Eurospin test objects and protocols. *Magn Reson Imaging* 1993;11:817–33.
- Wang Y, Riederer SJ, Ehman RL. Respiratory motion of the heart: kinematics and the implications for the spatial resolution in coronary imaging. *Magn Reson Med* 1995;33:713–9.
- McGee KP, Manduca A, Felmlee JP, Riederer SJ, Ehman RL. Image metric-based correction (autocorrection) of motion effects: analysis of image metrics. *J Magn Reson Imaging* 2000;11:174–81.
- Hundley WG, Bluemke DA, Finn JP, Flamm SD, Fogel MA, Friedrich MG, et al. ACCF/ACR/AHA/NASCI/SCMR 2010 expert consensus document on cardiovascular magnetic resonance: a report of the American College of Cardiology foundation task force on expert consensus documents. *Circulation* 2010;121:2462–508.
- Lintingre P-FF, Nivet H, Clément-Guinaudeau S, Camaioni C, Sridi S, Corneloup O, et al. High-resolution late gadolinium enhancement magnetic resonance for the diagnosis of myocardial infarction with nonobstructed coronary arteries. *JACC Cardiovasc Imaging* 2020;13:1135–48.
- Di Marco A, Anguera I, Schmitt M, Klem I, Neilan T, White JA, et al. Late gadolinium enhancement and the risk for ventricular arrhythmias or sudden death in dilated cardiomyopathy: systematic review and meta-analysis. *JACC Hear Fail* 2017;5:28–38.
- Muscogiuri G, Gatti M, Dell'aversana S, Guaricci AI, Guglielmo M, Baggiano A, et al. Image quality and reliability of a novel dark-blood late gadolinium enhancement sequence in ischemic cardiomyopathy. *J Thorac Imaging* 2020;35:326–33.
- Foley JR, Broadbent DA, Fent GJ, Garg P, Brown LAE, Chew PG, et al. Clinical evaluation of two dark blood methods of late gadolinium quantification of ischemic scar. *J Magn Reson Imaging* 2019;50:146–52.
- Basha TA, Tang MC, Tsao C, Tschabrunn CM, Anter E, Manning WJ, et al. Improved dark blood late gadolinium enhancement (DB-LGE) imaging using an optimized joint inversion preparation and T2 magnetization preparation. *Magn Reson Med* 2018;79:351–60.